

Dynamical analysis of low-energy electron diffraction intensities from GaAs(110)- $p(1 \times 1)$ -Sb(1ML)

C. B. Duke, A. Paton, and W. K. Ford

Xerox Webster Research Center, Xerox Square-W114, Rochester, New York 14644

A. Kahn and J. Carelli

*Department of Electrical Engineering and Computer Science, Princeton University,
Princeton, New Jersey 08544*

(Received 18 February 1982)

The deposition of Sb on GaAs(110) at room temperature produces a stable, ordered, saturated adsorbate structure at a coverage of approximately one monolayer (1 ML, i.e., one Sb for each Ga and As surface species). An analysis of the atomic geometry of this GaAs(110)- $p(1 \times 1)$ -Sb(1 ML) overlayer system was performed by the comparison of dynamical calculations of elastic low-energy electron diffraction (LEED) intensities with those measured at room temperature. A nonrelativistic model embodying energy-independent Slater exchange was utilized in the analysis to achieve compatibility with previous studies of the GaAs(110) substrate. Five qualitatively distinct classes of geometrical models were examined, each corresponding to a different hypothesis concerning the nature of the Sb-GaAs chemical bond. Only one of these, a model in which the Sb adsorbates occupy sites corresponding to both the Ga and As species on the surface of unrelaxed GaAs(110), provided a reasonable description of the measured LEED intensities. Refinement of this class of structures led to a best-fit atomic geometry which provides a description of the LEED intensity data comparable to that achieved for the clean (110) surfaces of compound semiconductors, i.e., GaAs(110), InSb(110), CdTe(110), InP(110), GaP(110), ZnS(110), and ZnTe(110). In this geometry, chains of Sb adsorbates characterized by an Sb-Sb bond length of 2.8 ± 0.1 Å reside upon a nearly unrelaxed GaAs(110) substrate. The Sb species bonded to the Ga substrate atoms lie 0.1 ± 0.075 Å above the Sb bonded to the substrate As. The Ga-Sb bond length is 2.6 ± 0.17 Å and the Sb-As bond length is 2.7 ± 0.17 Å. The uppermost As in the substrate is relaxed toward the bulk GaAs by 0.1 Å relative to the uppermost Ga, which retains its bulk (i.e., unrelaxed) position relative to the substrate. This structure corresponds to bond angles of approximately 104° between the Sb adsorbates and the substrate species to which they are bonded and to bond angles of 91° between the Sb species in the zigzag overlayer chain. It constitutes a saturated monolayer because the valence of each adsorbed Sb is completely satisfied with two electrons participating in the nearest-neighbor bonds, one in the bond to the substrate, and the other two occupying the lone-pair charge density corresponding to the missing bond directed out of the surface.

INTRODUCTION

Interest in the structure formed when Sb is adsorbed on the (110) surface of GaAs was kindled by the photoemission and low-energy electron diffraction (LEED) studies of Skeath *et al.*^{1,2} These authors recognized that for room temperature adsorption the Sb forms an ordered overlayer structure with the same symmetry as the clean GaAs(110) surface [i.e., a $p(1 \times 1)$ structure] at approximately monolayer coverage. They proposed several different atomic geometries for these Sb overlayers,² but were unable to distinguish between

the hypothetical model geometries on the basis of their photoemission and fragmentary LEED data. As they stressed, however, the determination of the character of the Sb bond to the GaAs substrate is important for the understanding of the growth of III-V semiconductors by molecular-beam epitaxy, especially since preliminary indications revealed considerable differences between the Sb-GaAs(110) system relative to its Al-GaAs(110) counterpart, the only adsorbate system on GaAs(110) for which the atomic geometries of ordered overlayers are known from LEED intensity analyses.^{3,4} Indeed, Skeath *et al.* utilized the presumed differences in

the nature of these two overlayer structures to develop a rationalization for the mechanism of molecular-beam epitaxy.²

The purpose of this paper is to report a determination by LEED intensity analysis of the atomic geometry of the ordered saturated adsorbate structure formed by one monolayer (1 ML) of Sb on GaAs(110), i.e., GaAs(110)-*p*(1×1)-Sb(1 ML). By comparing LEED intensities calculated for various hypothetical geometries with the intensities measured at room temperature, we are able to demonstrate decisively the superiority of one narrow range of geometries relative to all the others which we examined. A schematic diagram of these geometries is shown in panel (a) of Fig. 1. The resulting structure is characterized by bond lengths characteristic of analogous bulk compounds, 91° bond angles between the Sb species in the zigzag overlayer chain, and bond angles in the range $102^\circ \leq \theta \leq 105^\circ$ between the adsorbates and the substrate species to which they are bonded. Thus, the directional (i.e., covalent) character of the Sb—substrate bond, anticipated by Skeath *et al.*,² is confirmed for the saturated monolayer structure.

We proceed by indicating our experimental procedures in Sec. II and defining our model calculations in Sec. III. We introduce in Sec. IV five classes of geometrical models associated with various distinct hypotheses about the nature of the chemical bonding of Sb to GaAs(110). The results of our structure analysis are presented in Sec. V. Since the experimental aspects of this work already have been presented elsewhere,^{5,6} our focus herein is on the structure analysis rather than the acquisition of the LEED intensity data.

II. EXPERIMENTAL PROCEDURES

All the experiments were performed in a standard UHV chamber at a background pressure of 2.0×10^{-10} Torr (2.6×10^{-8} Pa) on both sputtered-annealed and cleaved *n*-type (Te-doped, $n = 5.0 \times 10^{17}$ cm⁻³) laser diode GaAs samples. The former type of samples as prepared from a polished wafer by sputtering for 10 min with 1-keV Ar ions and then annealing at 550°C for 1 h. Sb was evaporated *in situ* from a Mo boat at a typical rate of 1–2 Å/min and a pressure lower than 4×10^{-10} Torr. Coverages were estimated by assuming a sticking coefficient of unity on GaAs(110) and were monitored by a Sloan Technology quartz-crystal oscillator. No substantial differences could be detected between the sputter-

annealed and cleaved surfaces.

The width of the interface was determined by evaporating increasing thicknesses of Sb on the surface and monitoring the adatom and substrate Auger electron peaks. The low- and high-energy Ga and As peaks decreased according to $e^{-z/\lambda}$, where z is the Sb thickness (2.7 Å/ML) and λ is the Auger escape depth. The values obtained for λ were 15 Å for the high-energy Ga (1065-eV) and As (1223-eV) peaks and 7 and 5.5 Å for the low-energy Ga (53-eV) and As (91-eV) peaks, respectively. These values indicate the formation of a continuous and homogeneous Sb film on the surface and suggest a sharp interface with no substantial Sb-substrate interdiffusion. This result is consistent with the ordered character of the interface as determined by LEED and the unlikelihood of an Sb-substrate replacement reaction because the heat of formation of GaSb is smaller than that of GaAs.

We also examined the desorption of Sb from GaAs and the stability of the interface under heat treatment. After a 40-Å overlayer was evaporated on the surface a series of 10-min annealing cycles was performed. The maximum annealing temperature of each cycle was progressively raised (125–760°C, 25°C steps) and Auger spectra were recorded after each cycle. Most of the Sb desorbed between 250 and 350°C, leaving on the surface the equivalent of 1 ML, as determined by comparison of the Auger electron spectroscopy (AES) peak ratios with those obtained from the deposition of 1 ML on the clean surface. The desorption of the remaining monolayer was slower and required higher temperature (550–760°C). Following this annealing procedure, synchrotron radiation core level spectroscopy⁵ revealed no chemical shifts of Ga 3*d*, As 3*d*, and Sb 4*d* relative to the as-deposited 1 ML of Sb. It did suggest, however, the existence of two inequivalent Sb species within the 1-ML structure, in agreement with the data of Skeath *et al.*^{1,2} LEED intensity profiles were measured with a spot photometer from the screen of a Varian four-grid LEED apparatus. Those from the annealed 1-ML—substrate interfaces exhibited no substantial differences with those measured from 1 ML evaporated on a cleaved surface.

The LEED intensity data were recorded with a Gamma Scientific Spot photometer and normalized to the incident beam current. The beams exhibited the (*hk*)=($\bar{h}\bar{k}$) symmetry for normally incident electrons just as in the case of clean GaAs(110). Two sets of room-temperature data were recorded.

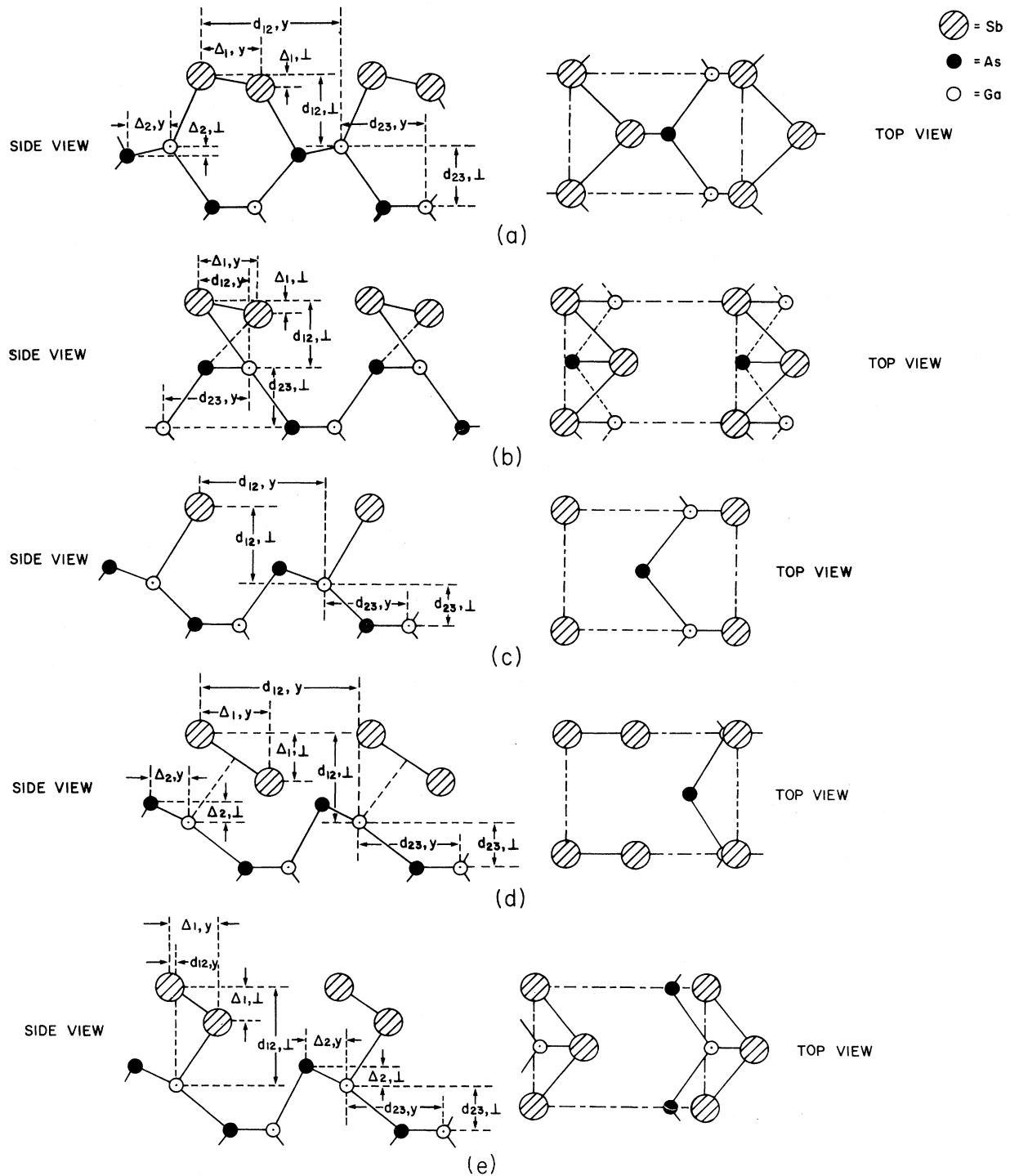


FIG. 1. Schematic diagrams of the five classes of surface geometries for GaAs(110)- $p(1 \times 1)$ -Sb(1 ML) which were considered in our structure analysis. (a): Models corresponding to approximate sp^3 bonding between the Sb and the substrate species. These emanate from the "model 2" structures of Skeath *et al.* (Ref. 2). (b): Overlapping-chain models corresponding to diffuse π bonding between the Sb chains in the overlayer and the GaAs chains in the (110) substrate. (c): Defect models corresponding to only one (ordered) Sb species per unit cell. (d): Dimer models corresponding to charge-exchange bonding between the π orbitals of Sb_2 and the empty p_z orbitals of the Ga in the top layer of the GaAs(110) substrate. (e): Models corresponding to p^3 bonding both within the Sb overlayer and between the Sb and the substrate. These are referred to as "Skeath model 1" following Skeath *et al.* (Ref. 2).

These were averaged in order to increase the signal-to-noise ratio. The intensity of each beam was corrected with a reference procedure to prevent artificial decrease due to slow surface contamination during the experiment: an important procedure for reactive AIs but almost unnecessary in the present case. Each of the five sets included 14 beams, i.e., those with the beam indices $(10)=(\bar{1}0)$, (01) , $(0\bar{1})$, $(11)=(\bar{1}\bar{1})$, $(\bar{1}\bar{1})=(\bar{1}\bar{1})$, (02) , $(0\bar{2})$, $(20)=(\bar{2}0)$, $(12)=(\bar{1}2)$, $(\bar{1}2)=(\bar{1}2)$, $(21)=(\bar{2}1)$, $(2\bar{1})=(\bar{2}\bar{1})$, $(13)=(\bar{1}3)$, and $(\bar{1}3)=(\bar{1}3)$. All intensities were measured in from 60 to 210 eV in 2-eV increments. Six of these beams, the (01) , $(0\bar{1})$, (11) , $(\bar{1}\bar{1})$, (12) , and (02) are much more intense than the rest. The $(\bar{1}2)$, (10) , and $(0\bar{2})$ beams are of medium intensity, whereas the (20) , (21) , $(2\bar{1})$, (13) , and $(\bar{1}3)$ beams are weak. We show plots comparing the calculated and measured intensity profiles only for the high- and medium-intensity beams, although all 14 beams are included in the R -factor analysis.^{7,8}

III. MODEL CALCULATIONS

An approximate multiple-scattering model of the diffraction process, described previously,⁹ was used to perform our dynamical calculations of the LEED intensities. In this model, which is embodied in a series of computer programs, the scattering species are represented by energy-dependent phase shifts in terms of which the LEED intensities from the surface are evaluated. The scattering amplitudes associated with the uppermost three atomic bilayers are evaluated exactly, as are those of each of the individual atomic layers beneath. These amplitudes are superposed, weighted by appropriate phase factors, to obtain the diffracted intensities. The accuracy of this calculational procedure has been verified in the analysis of several zinc-blende (110) surfaces, specifically GaAs(110) and ZnTe(110), for which the intensity profiles calculated solving the scattering in the uppermost four atomic bilayers exactly were compared with those calculated solving the scattering in the uppermost three bilayers exactly. Convergence tests revealed that the consideration of a slab of six atomic layers and the use of six phase shifts for each scatterer yield predicted intensities which are generally accurate to within a few percent, so these parameters were adopted for the calculations presented herein.

The electron-ion-core interaction is described by a one-electron muffin-tin potential. The one-

electron crystal potential is formed from a superposition of overlapping atomic charge densities (i.e., neutral Sb, As, and Ga). These charge densities are obtained via self-consistent solutions to the Schrödinger equation for the individual atomic species. Given the charge densities, the phase shifts are evaluated by solving the Schrödinger equation using the Slater model for the exchange potential.^{10,11} A muffin-tin approximation to the crystal potential is imposed prior to the calculation of the phase shifts. The muffin-tin radii are taken to be the values at which the potentials of two Sb species in a GaAs lattice cross for the top-layer Sb and at which the Ga and As potentials cross for the substrate species. These radii are $r_{\text{MT}}(\text{Sb}) = 1.22 \text{ \AA}$, $r_{\text{MT}}(\text{As}) = 1.25 \text{ \AA}$, and $r_{\text{MT}}(\text{Ga}) = 1.19 \text{ \AA}$, for the Sb, As, and Ga species, respectively. The value of the potential outside these radii within a Wigner-Seitz cell is taken to be a constant value equal to the average value of the atomic potential outside the muffin-tin spheres but within the Wigner-Seitz cell. The resulting phase shifts are shown in Fig. 2. We verified that the phase shifts for neutral Ga and As obtained by using this procedure are essentially identical to the Ga^+ and As^- phase shifts used in our earlier analysis of the atomic geometry of clean GaAs(110).⁹ Therefore, the phase shifts used herein are explicitly compatible with those used both for the substrate alone⁹ and for the chemisorption of Al on GaAs(110).^{3,4} The total elastic scattering cross sections predicted by these phase shifts for the Sb, As, and Ga scatterers are shown in Fig. 3.

The electron-electron interaction is incorporated into our model via a complex inner potential with constant real part V_0 and an imaginary part characterized by the inelastic collision mean free path λ_{ee} .¹² We select V_0 to minimize the x-ray R factor¹³ [given by Eqs. (3), (8), (13), (14), and (16) of Ref. 13]. Our major structure searches were performed using $\lambda_{ee} = 8 \text{ \AA}$, although we examined the sensitivity of the values of the R factor to the value of λ_{ee} .

The consequences of thermal lattice vibrations are neglected in the structure search reported herein, because previous studies of their consequences for GaAs(110) (Ref. 9) and GaP(110) (Ref. 7) revealed that incorporation of bulk lattice vibrations into the model did not affect the results of the structure analysis. While it is possible that inclusion of the difference between the bulk and surface vibrational amplitudes could influence our results for the Sb overlayer system, we did not exam-

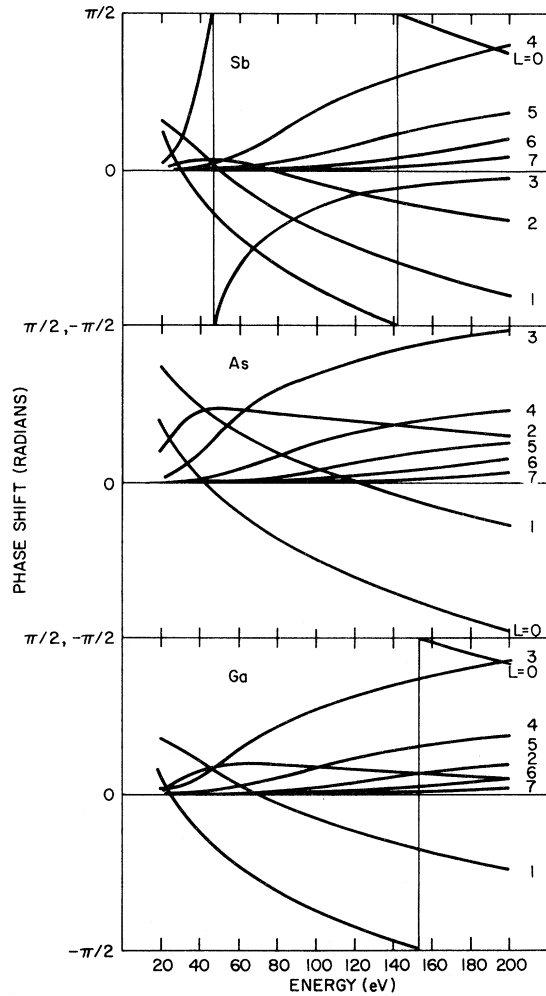


FIG. 2. Phase shifts for the Sb, As, and Ga species resulting from Slater exchange. These phase shifts were obtained using the muffin-tin radii $r_{MT}(\text{Sb})=1.22 \text{ \AA}$, $r_{MT}(\text{As})=1.25 \text{ \AA}$, $r_{MT}(\text{Ga})=1.19 \text{ \AA}$ and the constant potentials $V(\text{Sb})=-21.44 \text{ eV}$, $V(\text{As})=-16.99 \text{ eV}$, and $V(\text{Ga})=-17.25 \text{ eV}$ outside the muffin-tin radii. The energy scales for each species are measured relative to the associated constant potential.

ine this issue because no estimates of the surface vibrational amplitudes are available.

IV. STRUCTURAL MODELS

Since little is known about the chemistry of Sb on GaAs, we performed our structure analysis utilizing a wide variety of geometrical models, each class of which corresponds to a possible mechanism for the interaction of gas phase Sb with the (reconstructed⁹) GaAs(110) surface. The five struc-

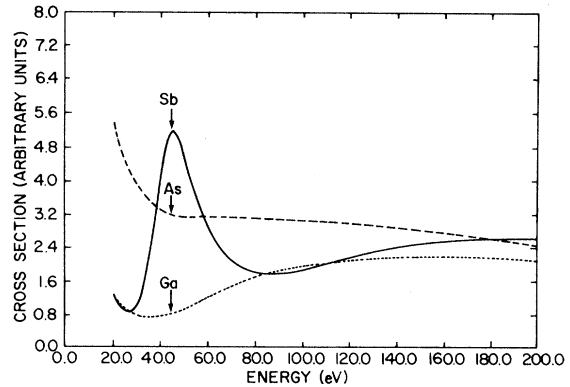


FIG. 3. Total elastic scattering cross sections (in arbitrary units) evaluated from the phase shifts shown in Fig. 2, of the Sb, As, and Ga scatterers. The energy scales are measured relative to the constant potential outside the muffin-tin radii as noted in the caption to Fig. 2.

tural classes which we considered are illustrated in panels (a)–(e) of Fig. 1; the associated best-fit variants thereof are specified in the corresponding panels of Table I, and the bond lengths characteristic of these best-fit geometries are given in Table II. This section is devoted to an indication of the nature of and motivation for each of these five types of structural model.

Perhaps the most obvious class of structural model, and the one which ultimately prevailed, is that defined by placing the two Sb species in the saturated monolayer at sites analogous to those which would have been occupied by Ga and As at an unreconstructed surface. Such a model would correspond to sp^3 bonding of the Ga and As substrate species to the Sb as well as of the Sb to each other if the Sb actually occupied the Ga and As sites. In this model, illustrated schematically in panel (a) of Fig. 1, the larger size of Sb relative to Ga and As is accommodated by expanding the Sb-Sb lateral spacing along the y axis (i.e., the horizontal axis in the right-hand panels of Fig. 1) in the GaAs(110) unit cell. The reflection symmetry of the surface unit cell must be retained in order to describe the observed $(hk)=(\bar{h}\bar{k})$ symmetry of the LEED spot pattern for normally incident electrons. Starting from the “pure sp^3 ” bonding model with the Sb at the Ga and As sites and relaxing both of the inequivalent Sb symmetrically along the y axis until the Sb-Sb bond length characteristic of bulk Sb is reached [$d(\text{Sb}-\text{Sb})=2.87 \text{ \AA}$] closes the bond angle between the Sb in the zigzag chain to $\theta(\text{Sb}-\text{Sb})\simeq 91^\circ$: a value approximately characteristic of p^3 bonding. This result immediately implies

TABLE I. Candidate structures for the surface atomic geometry of GaAs(110)- $p(1 \times 1)$ -Sb(1 ML). The structural symbols Δ and d are defined in Fig. 1. The inner potential V_0 , as well as the x-ray R factor R_x is defined in the text. $\lambda_{ee} = 8 \text{ \AA}$ for all the calculated R factors in the table.

Structure	$\Delta_{1,1}$ (\AA)	$\Delta_{1,y}$ (\AA)	$d_{12,1}$ (\AA)	$d_{12,y}$ (\AA)	$\Delta_{2,1}$ (\AA)	$\Delta_{2,y}$ (\AA)	$d_{23,1}$ (\AA)	$d_{23,y}$ (\AA)	R_x	V_0 (eV)
(a) best fit	0.10	1.96	2.39	4.62	0.10	1.41	2.00	2.83	0.20	10
(b) overlapping chain	0.10	1.96	2.19	1.62	0.00	1.41	2.00	2.83	0.30	9
(c) defect ($\frac{1}{2}$ ML)			2.54	4.14	0.50	1.41	1.42	2.83	0.36	10
(d) Sb ₂ dimer	1.60	2.30	2.97	5.29	0.65	1.26	1.49	3.31	0.42	1
(e) skeath model 1 (“ p^3 ” chain)	1.12	1.61	3.29	0.09	0.65	1.26	1.49	3.31	0.51	7

that the plane of the zigzag chain of Sb is not parallel to that of the GaAs surface because some hybridization of the p orbitals in the plane of the chain with that normal to the chain must occur in order to bond with the “dangling bonds” of an unreconstructed GaAs substrate. Moreover, the necessity of such a structure further implies some reconstruction of the substrate so that the Ga and As are not equivalent. Since it is not obvious *a priori* how much hybridization of the Sb chain p orbitals occurs, however, we started our search with a symmetrical structure characterized with $d(\text{Sb}-\text{Sb}) = 2.87 \text{ \AA}$ and $d(\text{Ga}-\text{Sb}) = d(\text{As}-\text{Sb}) = 2.65 \text{ \AA}$, the latter being characteristic of bulk GaSb. In this model, three of the Sb electrons participate in bonds and two occupy a s - p hybrid lone-pair charge density which is analogous to the charge density for bonding to the substrate species but pointing out of the surface. Such bonding is similar to that of S₈ and Se₈.¹⁴ Thus, the valences of both surface Sb species are fully saturated at monolayer coverage and the main driving force for the reconstruction of the GaAs(110) substrate is eliminated by the Sb-substrate bonding. The starting model (but not the final optimized structure) is

TABLE II. Bond lengths associated with the best fit structures for GaAs(110)- $p(1 \times 1)$ -Sb(1 ML) specified in Table I and Fig. 1.

Structure	Ga—Sb	Sb—Sb	Sb—As
(a)	2.61	2.80	2.70
(b)	2.73	2.80	2.73
(c)	2.70		
(d)	3.00 ^a	2.80	
(e)	2.65	2.80	2.89

^aBoth Sb are equidistant from Ga.

essentially identical to “Sb chain model 2” proposed by Skeath *et al.*² in their analysis of photoemission data, although these authors seemed to prefer the p^3 bonding model discussed below.

The p^3 structure proposed by Skeath *et al.* is referred to as “model 1” in their paper² and is obtained by presuming that one of the Sb species exhibits p^3 bonding both to the substrate Ga and to two neighboring Sb species in a zigzag chain. The resulting structure is illustrated in panel (e) of Fig. 1 and specified in panel (e) of Table I. The valences of the two Sb species in this structure presumably are satisfied by virtue of the Sb which is bound to the Ga exhibiting a formal excess electron obtained from the second Sb species. The first Sb contributes two electrons to its p bond with the Ga, one each to its p bonds with the two neighboring Sb, and two to a lone-pair s -electron charge density. The second Sb contributes one electron to each of its two p bonds with neighboring Sb species of the first kind, and two electrons to a lone-pair s -electron charge density. The GaAs(110) substrate remains reconstructed so that the surface Ga have empty p orbitals to accept the charge donated from the Sb to which they are bound. It is not self-evident that such a structure would be saturated at monolayer coverage because the second Sb species could accept charge from an additional Sb in a subsequent layer. Hence the adsorption process could continue, resulting in a multilayer structure, as recognized by Skeath *et al.*² Consequently, we regard this model as being incompatible with the results of our thermal desorption studies.^{5,6} As we shall see in Sec. V, it also is incompatible with the measured LEED intensity profiles at normal incidence.

If instead of considering local atomic bonding between the Sb and substrate species one envisages

delocalized (e.g., π) bonding between a zigzag chain of Sb adsorbates and the Ga-As chains in the uppermost layer of the GaAs(110) substrate, the model indicated in panel (b) of Fig. 1 is suggested. In our initial version of this model the zigzag Sb chain is regarded as exhibiting approximate sp^2 bonding, with each Sb contributing one electron to a sigma bond with each of its two neighbors, two electrons to a lone-pair sp^2 -like electron charge density in the plane of the chain, and one electron to a delocalized π bond along the chain. This π bond in turn can experience charge exchange with the low-energy delocalized empty surface state orbitals associated with GaAs(110), probably inducing its reconstruction to diminish in order to reduce the energy of the lowest empty orbital.¹⁵⁻¹⁹ Such a structure would exhibit nonmetallic electronic behavior because the two Sb species in the chain are electronically inequivalent owing to their different bonding to the substrate. Our initial calculations based on this model gave poor R factors, presumably because of the short Sb-Sb bond lengths implied by the combination of the large (120°) Sb-Sb-Sb bond angles in the zigzag chain and the requirement that each pair of Sb species in the chain must fit into the GaAs(110) unit cell. Reducing the Sb-Sb-Sb bond angle by moving the Sb apart along the y axis (i.e., the horizontal axis in Fig. 1) for both Sb species approximately 2.4 Å above an unreconstructed substrate yielded a monotonic decrease in the R factor until a minimum at an Sb-Sb-Sb bond angle of 91° was reached. The resulting structure was then refined to give the best-fit "overlapping chain" geometry specified in panel (b) of Tables I and II. As evident from Table I, a marginally acceptable description of the measured LEED intensities can be achieved by the resulting "overlapping chain" model in which the intrachain bond angles in the Sb chain are in the vicinity of 90° , whereas those in the underlying Ga-As chain are in the vicinity of 104° .

Another type of delocalized electron charge transfer bonding can be visualized between the highest occupied (π) orbitals of Sb_2 dimers and the empty surface states derived predominantly from the p_z orbitals of the Ga species on reconstructed GaAs(110). This type of bonding corresponds to structures like that illustrated in panel (d) of Fig. 1. Such atomic geometries lead to saturated monolayers in which the two Sb species are inequivalent as required by the photoemission data. We were unable to find a region of geometrical parameters

which rendered them compatible with the LEED intensity data, however, as indicated by the "best-fit" structure specified in panel (d) of Table I.

A final class of structures which we considered is defined by half monolayer coverage of atomic Sb bonded to the Ga in GaAs(110). These geometries are indicated in panel (c) of Fig. 1. Their examination was motivated both by the inevitable uncertainties in specifying the absolute surface coverage (i.e., could the saturated structure actually occur at 0.5-ML coverage?) and by the possibility that one adsorbed Sb species was ordered but the second one was disordered at room temperature. In spite of encouraging preliminary indications from kinematical analyses,⁶ this class of structures did not yield a satisfactory dynamical description of the measured LEED intensities, as may be discerned from panel (c) of Table I in which the results are presented for the best-fit structure of this class.

V. LEED INTENSITY ANALYSIS

For each of the five classes of structures specified in Fig. 1 and Sec. IV an extensive structural search was performed. Starting from reference structures embodying our initialized bond lengths [$d(\text{Sb-Sb})=2.87$ Å, $d(\text{Ga-Sb})=2.65$ Å, $d(\text{As-Sb})=2.65$ Å], we varied the vertical heights of the two Sb species above the surface in order to search for minima in the x-ray R factor R_x as a function of these two variables. If this minimum yielded $R_x \leq 0.3$, we refined the structure further by varying the y component of the Sb-Sb bond length (i.e., the Sb-Sb separation in the horizontal direction in the right-hand column of Fig. 1). The x component of the Sb-Sb bond length (i.e., the Sb-Sb separation in the vertical direction in the right-hand column of Fig. 1) is fixed at $a_x[\text{GaAs}(110)]/2=2.00$ Å by the symmetry of the LEED diffraction pattern in structures (a), (b), and (e). For the atomic (c) and dimer (d) structures, the x component of the Sb-Sb spacing is fixed at $a_x[\text{GaAs}(110)]=4.00$ Å by this symmetry. In both cases this value represents a next-nearest-neighbor rather than nearest-neighbor spacing. For the initial searches, the substrate was taken to be unreconstructed for structures (a) and (b). For structures (c)-(e), it was taken to exhibit its vacuum reconstruction.⁹ Variations in the substrate reconstruction were examined only if the initial search yielded $R_x \leq 0.3$.

For each structure which we considered, the

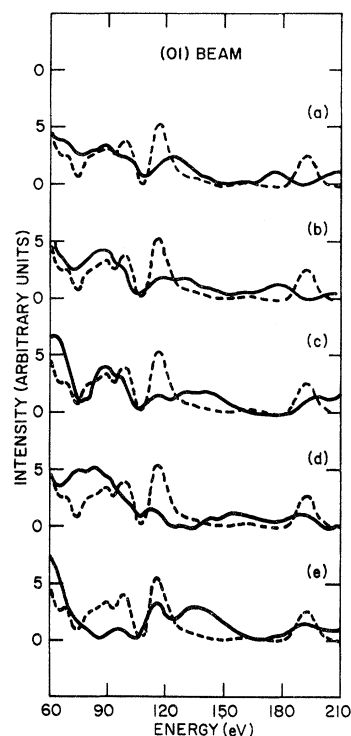


FIG. 4. Comparison of the calculated (solid lines) and measured (dashed lines) intensities of electrons normally incident on GaAs(110)- $p(1 \times 1)$ -Sb(1 ML) diffracted into the (01) beam. (a): Calculated intensities for the overall best-fit structure as specified in panel (a) of Table I and Fig. 1. This structure corresponds to approximate sp^3 bonding of the adsorbed Sb to the nearest-neighbor substrate species. It is an extension of model 2 of Skeath *et al.* (Ref. 2). (b): Calculated intensities for the overlapping chain model, specified in panel (b) of Table I and Fig. 1, which provided the best description of the measured intensities. (c): Calculated intensities for the single Sb defect model, specified in panel (c) of Table I and Fig. 1, which provided the best description of the measured intensities. (d): Calculated intensities for the Sb_2 dimer model; specified in panel (d) of Table I and Fig. 1, which provided the best description of the measured intensities. (e): Calculated intensities for the p^3 bonding model of Skeath *et al.* (Ref. 2) specified in panel (e) of Table I and Fig. 1.

LEED intensities for normally incident electrons in the energy range $60 \text{ eV} \leq E \leq 210 \text{ eV}$ were calculated and compared via an x-ray R -factor analysis with the intensities measured for the 14 beams noted in Sec. II. Over 150 model structures were examined in this fashion. The resulting comparisons between the calculated and measured LEED inten-

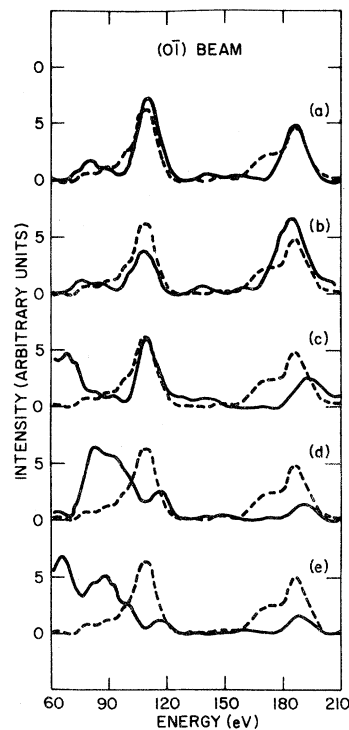


FIG. 5. Same as Fig. 4 for the (0 $\bar{1}$) beam.

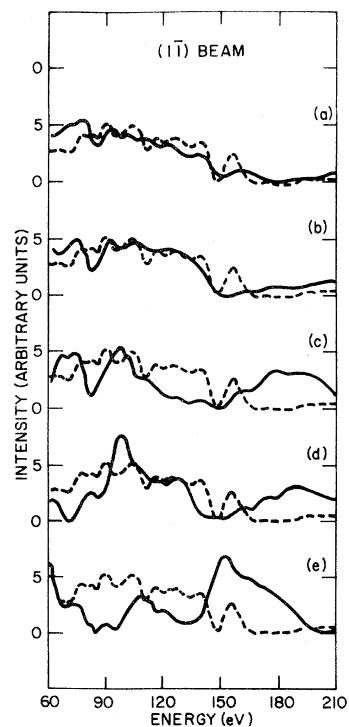


FIG. 6. Same as Fig. 4 for the (1 $\bar{1}$) beam.

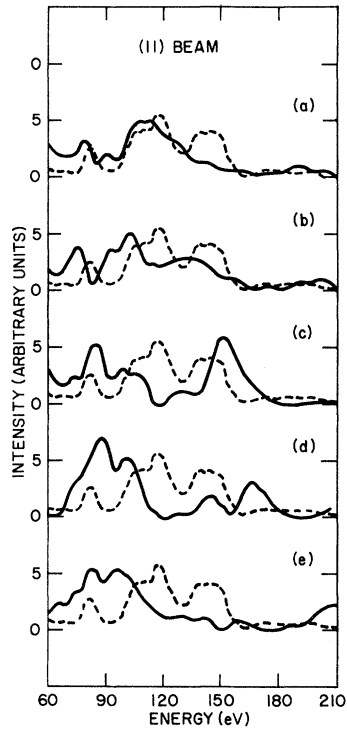


FIG. 7. Same as Fig. 4 for the (11) beam.

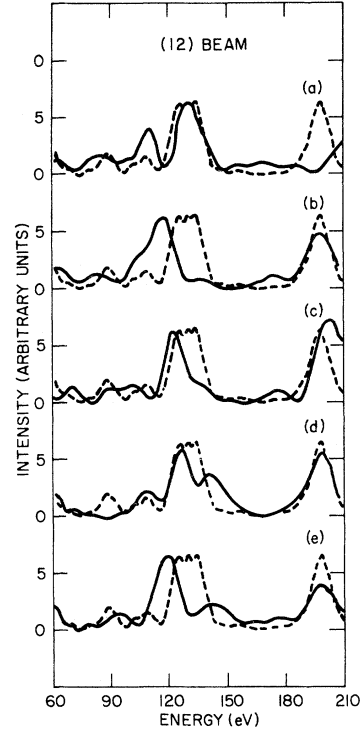
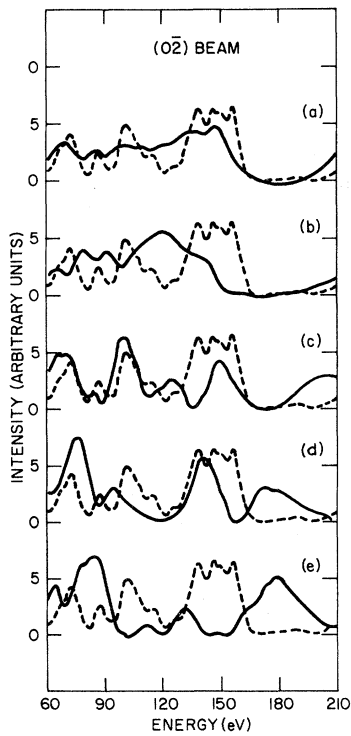
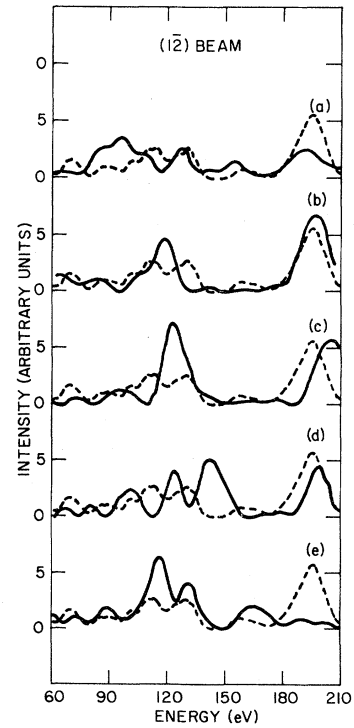


FIG. 9. Same as Fig. 4 for the (12) beam.

FIG. 8. Same as Fig. 4 for the $(0\bar{2})$ beam.FIG. 10. Same as Fig. 4 for the $(\bar{1}2)$ beam.

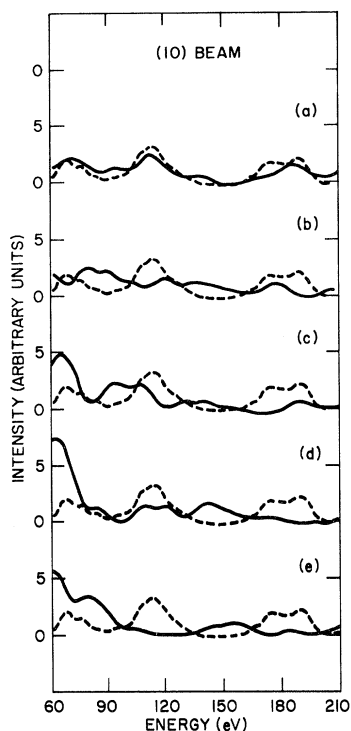


FIG. 11. Same as Fig. 4 for the (10) beam.

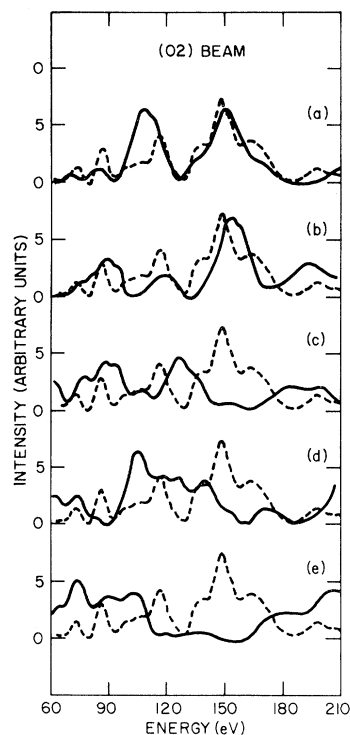


FIG. 12. Same as Fig. 4 for the (02) beam.

sities are shown in Figs. 4–12 for the “best-fit” structure in each class of models. These structures are specified in Fig. 1 and Tables I and II. The ranges of parameters searched for in each class of structures are indicated in Table III. The comparisons shown in Figs. 4–12 are presented in order of decreasing integrated beam intensity from the most intense beam [$I(01)=439$ in arbitrary units] to the weakest “medium” beam [$I(02)=85$ a.u.]. The strongest beam not shown is $I(21)=52$ a.u., i.e., roughly half as intense as the (02) beam and an

order of magnitude less intense than the (01) beam.

Our original searches revealed that structures in classes (a)–(c) *might* be compatible with the LEED intensity data whereas those in classes (d) and (e) clearly are not. This result for the latter two classes of structure is evident from Table I and Figs. 4–12 in which the results for the best candidates in these classes are presented. Refinement of the initial structures in classes (b) and (c) failed, however, to reveal any which provided a truly satisfactory description of the measured LEED inten-

TABLE III. Range of structural parameters for the Sb overlayer searched in order to obtain the “best-fit” GaAs(110)- $p(1\times 1)$ -Sb(1 ML) geometries specified in Fig. 1 and in Tables I and II. Most of the searches were performed for both unreconstructed and a range of reconstructed GaAs(110) substrates.

Structure	$\Delta_{1,1}$	$d_{12,1}$	$d_{12,y}$
(a) “ sp^3 ” chain	(-1.45, +1.20)	(1.81,3.40)	(3.92,4.72)
(b) overlapping chain	(-0.10, +0.20)	(1.99,2.19)	(1.22,1.75)
(c) defect		(2.14,2.74)	4.14
(d) Sb_2 dimer	(0.60, +1.60)	(2.33,3.78)	(4.14,6.97)
(e) Skeath model 1 (“ p^3 ” chain)	(-0.80, +1.15)	(2.20,3.46)	(-2.83, +1.96)

sities, although each of the corresponding best-fit structures affords an adequate description of a few beams [e.g., (01), (1 $\bar{1}$), and (02) for class (b); (0 $\bar{2}$) and (12) for class (c)]. Thus, by elimination, only the class (a) ("Skeath model 2") models seem compatible with the LEED intensity data.

Plots of R_x as a function of the three independent overlayer structural variables are shown in Fig. 13 for structures in the vicinity of the best-fit atomic geometry specified by panel (a) in Table I. The minimum in R_x as a function of each of three variables is sharply defined with an estimated precision ($\Delta R_x=0.02$) of 0.075, 0.1, and 0.15 Å in $\Delta_{1,1}$, $d_{12,1}$, and $\Delta_{1,y}$ respectively. The estimated absolute accuracies [$\Delta R_x=0.04$ (Refs. 7 and 8)] are 0.11, 0.16, and 0.22 Å, respectively. The minimum value of R_x , i.e., $R_x(\text{min})=0.20$ for $\lambda_{ee}=8$ Å and $R_x(\text{min})=0.18$ for $\lambda_{ee}=10$ Å, compares favorably with the values obtained for GaAs(110) [$R_x(\text{min})=0.14$], GaP(110) [$R_x(\text{min})=0.17$],⁷ CdTe(110) [$R_x(\text{min})=0.18$],⁸ InP(110) [$R_x(\text{min})=0.17$],²⁰ InSb [$R_x(\text{min})=0.16$],²⁰ ZnTe(110) [$R_x(\text{min})=0.25$],²⁰ and ZnS [$R_x(\text{min})=0.22$].²¹ Therefore we may be confident that the atomic geometry given in panel (a) of Table I is compatible with our LEED intensity data as well as with existing photoemission^{1,2} and thermal desorption^{5,6} measurements. An important and well-established feature of this atomic geometry is the 0.1 Å upward displacement of the Sb bound to the substrate Ga relative to the Sb bound to the substrate As. This is accompanied by a comparable upward displacement of the Ga relative to the As in the uppermost layer of the substrate.

VI. SYNOPSIS

Analysis of measured room-temperature LEED intensities from GaAs(110)- $p(1\times 1)$ -Sb(1 ML) via

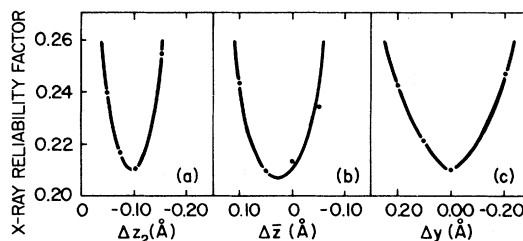


FIG. 13. Variation of x-ray reliability factor with various structural parameters. (a): Vertical displacement of Sb2 (bonded to As) relative to Sb1 (bonding to Ga) with Sb1 being fixed at 2.39 Å above an unreconstructed substrate. (b): Vertical displacement of the midpoint of the Sb bilayer relative to one in which Sb1 is 2.44 Å above an unreconstructed substrate and Sb2 is 0.10 Å below Sb1. (c): Change in horizontal (y) displacement of Sb1 and Sb2 relative to a reference structure in which Δy is 1.95 Å. Sb1 and Sb2 are fixed at heights at 2.39 and 2.29 Å, respectively, above an unreconstructed substrate.

dynamical calculations of these intensities reveals only one region of surface atomic geometries which lead to an adequate description of the intensity data. This region consists of the structures specified by panel (a) in Table I and Fig. 1 with uncertainties of 0.11 Å in $\Delta_{1,1}$, 0.16 Å in $d_{12,1}$, and 0.22 Å in $\Delta_{1,y}$. The uncertainties in the substrate positions are not readily established, but the small reconstruction specified in panel (a) of Table I is clearly preferred over an unreconstructed substrate. The nature of the bonding associated with this structure is described in Sec. IV.

ACKNOWLEDGMENTS

The authors are indebted to L. J. Kennedy for assistance and Dr. M. D. Tabak for his generous support of this work.

¹P. Skeath, C. Y. Su, I. Lindau, and W. E. Spicer, *J. Vac. Sci. Technol.* **17**, 874 (1980).
²P. Skeath, I. Lindau, C. Y. Cu, and W. E. Spicer, *J. Vac. Sci. Technol.* **19**, 556 (1981).
³C. B. Duke, A. Paton, R. J. Meyer, L. J. Brillson, A. Kahn, D. Kanani, J. Carelli, J. L. Yeh, G. Margaitondo, and A. D. Katnani, *Phys. Rev. Lett.* **46**, 440 (1981).
⁴A. Kahn, J. Carelli, D. Kanani, C. B. Duke, A. Paton, and L. J. Brillson, *J. Vac. Sci. Technol.* **19**, 331

(1981).
⁵J. Carelli and A. Kahn, *Surf. Sci.* **116**, 380 (1982).
⁶A. Kahn, J. Carelli, C. B. Duke, A. Paton, and W. K. Ford, *J. Vac. Sci. Technol.* **20**, 775 (1982).
⁷C. B. Duke, A. Paton, W. K. Ford, A. Kahn, and J. Carelli, *Phys. Rev. B* **24**, 562 (1981).
⁸C. B. Duke, A. Paton, W. K. Ford, A. Kahn, and G. Scott, *Phys. Rev. B* **24**, 3310 (1981).
⁹R. J. Meyer, C. B. Duke, A. Paton, A. Kahn, E. So, J. L. Yeh, and P. Mark, *Phys. Rev. B* **19**, 5194 (1979).

- ¹⁰J. C. Slater, *Phys. Rev.* **81**, 385 (1951).
- ¹¹C. B. Duke, N. P. Lipari, and U. Landman, *Phys. Rev. B*, **8**, 2454 (1973).
- ¹²C. B. Duke, *Adv. Chem. Phys.* **27**, 1 (1974); in *Dynamic Aspects of Surface Physics, Proceedings of the International School of Physics "Enrico Fermi,"* edited by F. O. Goodman (Editrice Compositori, Bologna, 1974), pp. 99–173.
- ¹³E. Zanazzi and F. Jona, *Surf. Sci.* **62**, 61 (1977).
- ¹⁴W. R. Salaneck, C. B. Duke, A. Paton, C. Griffiths, and R. C. Keezer, *Phys. Rev. B* **15**, 1100 (1977).
- ¹⁵J. R. Chelikowsky, S. G. Louie, and M. L. Cohen, *Phys. Rev. B* **14**, 4724 (1976).
- ¹⁶C. Calandra, F. Manghi, and C. M. Bertoni, *J. Phys. C* **10**, 1911 (1977).
- ¹⁷E. J. Mele and J. D. Joannopoulos, *Surf. Sci.* **66**, 38 (1977); *Phys. Rev. B* **17**, 1816 (1978).
- ¹⁸A. Zunger, *Phys. Rev. B* **22**, 959 (1980).
- ¹⁹D. J. Chadi, *J. Vac. Sci. Technol.* **15**, 631 (1978); *Phys. Rev. B* **18**, 1800 (1978).
- ²⁰W. K. Ford, C. B. Duke, and A. Paton, *Surf. Sci.* **115**, 195 (1982).
- ²¹C. B. Duke, R. J. Meyer, A. Paton, A. Kahn, J. Carelli, and J. L. Yeh, *J. Vac. Sci. Technol.* **18**, 866 (1981).